FERMILAB
APR 26 1996
LIBRARY

DFUB 96/10

FIRST RESULTS FROM THE LEP RUN AT $\sqrt{s}$ = 130–140 GeV

G. GIACOMELLI
Dipartimento di Fisica, Università di Bologna and INFN, Bologna, Italy
CERN, Geneva, Switzerland

and

P. GIACOMELLI
Department of Physics, University of California at Riverside, California, USA
CERN, Geneva, Switzerland

Invited paper at the QMatic Conf., Dera Ismail Khan, Pakistan

DFUB 96-10
Fermilab Library
0 1160 0042459 2

Abstract

After a brief summary of the results obtained at LEP1 ($\sqrt{s} \simeq 90$ GeV), the recent results obtained at LEP1.5 ($\sqrt{s}$ = 130–140 GeV) are presented and discussed.

1. Introduction

From August 1989 until October 1995, the LEP positron–electron collider was working at energies at or around the Z^0 mass (this phase is usually called LEP1 or LEP100). During this period, each of the four experiments at LEP (ALEPH, DELPHI, L3 and OPAL) recorded about 5 million events, corresponding to an integrated luminosity of about 170 pb^{-1}. Accurate measurements of the Z^0 mass, width and decay properties are precision tests of the electroweak theory. The results are summarized in Table 1. Note the high precision in the Z^0 mass, width and height measurements, which required unprecedented accuracy in the determination of the LEP luminosity (to within about 0.1%), and corrections for the moon's orbit, the water level in Lac Léman and the passage of French high-speed trains! Note that the radiative corrections lead to the determination of the top-quark mass below threshold, yielding a value which agrees perfectly with the recent directly measured value. By a similar procedure, it is hoped to be able to roughly determine the Higgs mass. Since the Z^0 decays predominantly into quark–antiquark pairs, it yields a clean data sample with which to test quantum chromodynamics (QCD, the theory of the strong interaction). Among the many results one may mention the running of α_s, its independence from the quark flavour, the proof of the non-abelian nature of QCD, the four-gluon vertex. A wealth of information has been obtained on hadron physics, measurements of short lifetimes, τ-physics, etc. Searches for new physics include those for supersymmetric particles, Higgs bosons,

substructures of quarks and leptons and tests for the validity of various conservation laws.

Table 1: Average electroweak parameters from the results of the four experiments at LEP1, assuming lepton universality.

Parameter	Average LEP	Standard Model
m_Z (MeV)	91188.4 ± 2.2	–
Γ_Z (MeV)	2496.3 ± 3.2	2497
σ_h^p (nb)	41.488 ± 0.078	41.45
$R_\ell = \Gamma_h/\Gamma_\ell$	20.788 ± 0.032	20.773
A_{FB}^ℓ	0.0172 ± 0.0012	0.0159
Γ_ℓ (MeV)	83.93 ± 0.14	83.4
Γ_h (MeV)	1744.8 ± 3.0	1734
Γ_{inv} (MeV)	499.9 ± 2.5	499
$A_\tau = -P_\tau$	0.1418 ± 0.0075	0.1455
A_e	0.1390 ± 0.0089	0.1455
R_b	0.2219 ± 0.0017	0.2156
R_c	0.1543 ± 0.0074	0.1724
$BR_\ell = \Gamma_\ell/\Gamma_Z$	3.36%	
BR_h	69.9%	
BR_{inv}	20.0%	

In November 1995 the LEP c.m. energy was raised to 130–140 GeV and data were taken by all experiments at $\sqrt{s} = 130$, 136 and 140 GeV with a total luminosity of about 5.5 pb^{-1} per experiment. These are the highest-energy e^+e^- collision data yet available and the first at energies well above the Z^0 resonance. On 12th December 1995, in four seminars at CERN, the four experiments presented preliminary results obtained during the runs at the new energies, collectively called LEP1.5 [1–4]. This paper is mainly based on these presentations (and on subsequent papers[5–8]). The data and the results presented at the seminars include measurements of the cross-sections and asymmetries for many channels, studies of QCD, tests of quantum electrodynamics (QED), searches for supersymmetric particles, study of specific channels (such as the four-fermion final states) and others.

A feature of e^+e^- collision data at these new c.m. energies is a tendency for radiative return to the Z^0, as illustrated in Fig. 1. If an initial-state radiation photon is emitted which reduces the effective c.m. energy of the subsequent e^+e^- collision, $\sqrt{s'}$, to the region of the Z^0 resonance, then the cross-section is greatly enhanced (the production of events with hard initial-state radiation is much higher than at LEP1). A distinction can be made between these radiative events and non-radiative events, for which $\sqrt{s'} \simeq \sqrt{s}$. The properties of the radiative data are expected to be similar to

those measured in Z^0 decays at LEP1, modified only by the boost due to recoil against hard initial-state radiations. The non-radiative data are expected to have somewhat different properties, reflecting in particular the substantially increased importance of photon exchange relative to Z^0 exchange.

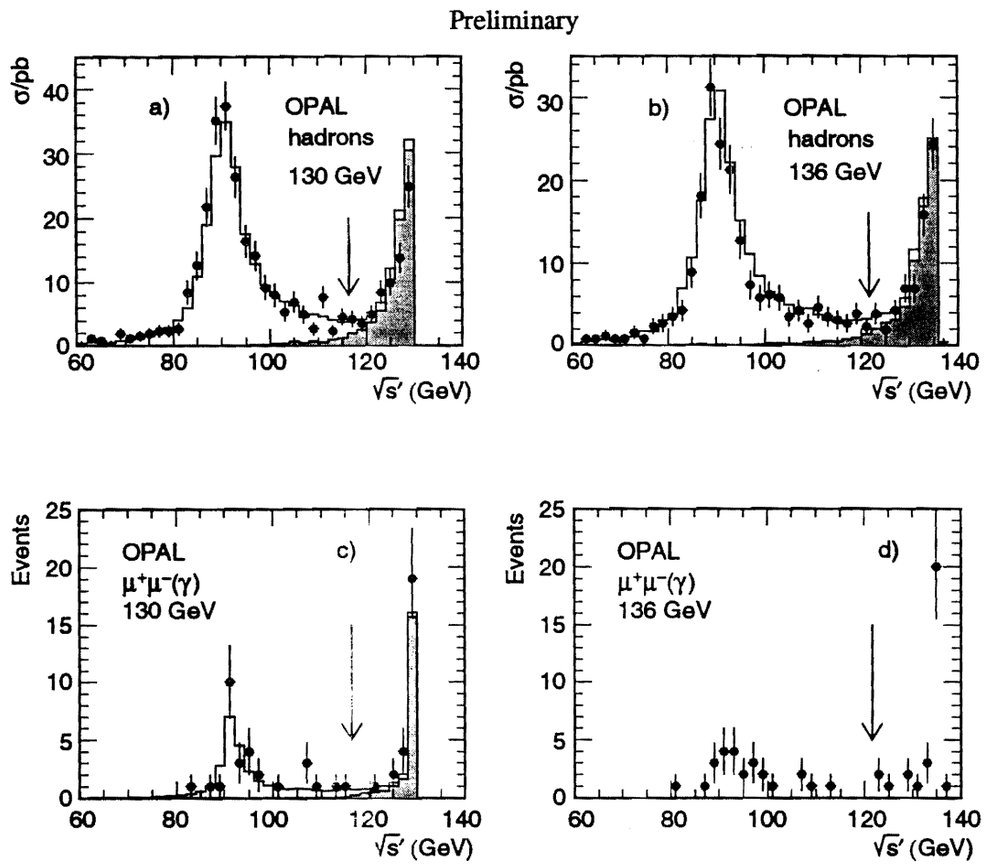

Figure 1: Distributions in $\sqrt{s'}$ at $\sqrt{s} = 130$ and 136 GeV for (a) and (b) hadronic events, and (c) and (d) muon pair events. The points are the data and the open histograms are the Monte Carlo predictions, with the shaded areas representing the predictions for events with $s'/s > 0.8$. The positions of the cuts used to separate non-radiative events are shown by arrows.

2. Experimental aspects

LEP is a circular e^+e^- collider with a circumference of 17 km, circulating beams of about 1 mA in four e^+ and four e^- bunches. The LEP1 era came to an end in the last week of September 1995. 16 new superconducting accelerating cavities were then installed in addition to the 44 already in LEP. At the end of October LEP was ready to start operation at 130–140 GeV (LEP1.5). The peak luminosity recorded at

LEP1.5 was around 10^{31} cm^{-2} s^{-1}. The data were recorded at c.m. energies of 130, 136 and 140 GeV with integrated luminosities per experiment of about 2.8, 2.9 and 0.05 pb^{-1}, respectively (corresponding in total to about 1500 multihadronic events per experiment).

Each of the four LEP detectors are 4π general-purpose experiments made up of several 'independent' subdetectors, whose combined role is to measure with high precision the energy, direction, charge and type of particles produced. The four experiments are being upgraded to better cover the forward angular range and to increase the acceptance of their microvertex detectors. Monte Carlo simulations were performed for the channels under study, processing the simulated samples through the full detector reconstruction.

The luminosity was measured via small-angle Bhabha scattering, $e^+e^- \to e^+e^-$, in the forward detectors. Typical precisions at LEP1.5 are $\lesssim 1.0\%$. This is adequate for the determination of all measured cross-sections, where precision is limited by the small amount of data currently available.

3. Cross-section measurements

Hadronic events. These were selected using criteria optimized at LEP1. The effective c.m. energy $\sqrt{s'}$ was estimated by attributing the observed hadrons to two jets with polar angles θ_1, θ_2; the energy of a possible undetected initial-state photon along the beam direction was estimated assuming three-body kinematics. In 20% of radiative events the photon was detected in the electromagnetic calorimeters. One could thus check the procedures and estimate the resolution in $\sqrt{s'}$ (about 2–3 GeV). The distributions in $\sqrt{s'}$ are shown in Fig. 1a–b; the predictions of the PYTHIA Monte Carlo are shown for comparison. The arrows indicate the cuts used in the distributions to separate radiative ($s'/s > 0.8$) from non-radiative ($s'/s < 0.8$) events. The total and the non-radiative hadron cross-sections, after corrections for acceptance and resolution, are shown in Fig. 2. The uncertainties ($> 3\%$) are mainly due to the small number of events in the selected samples.

e^+e^- final states. The selection of e^+e^- final states is based on the information from the E.M. calorimeters with the cut $\theta_{\rm acol} < 10°$ (which corresponds to $s'/s > 0.8$) and in $|\cos\theta_e|$. Three samples were selected corresponding to $|\cos\theta_e < 0.7, 0.8$ and 0.96, respectively. The distributions in $\sqrt{s'}$ for the first sample are shown in Fig. 1c–d. At these energies the selected e^+e^- samples, in particular that for $|\cos\theta_e| < 0.96$, are dominated by the QED t-channel scattering diagram, giving a strongly forward-peaked $\cos\theta_e$ distribution. For the $|\cos\theta_e| < 0.7$ sample the $\sqrt{s'}$ distribution (Fig. 1c–d), the cross-sections (Fig. 2c–d) and the asymmetries at both $\sqrt{s} = 130$ and 136 GeV are computed. The average of the asymmetries at $\sqrt{s} = 133$ GeV is $A_e = 0.77 \pm 0.04$, which agrees with the predictions of the ALIBABA Monte Carlo, as do the cross-sections of Fig. 2c–d.

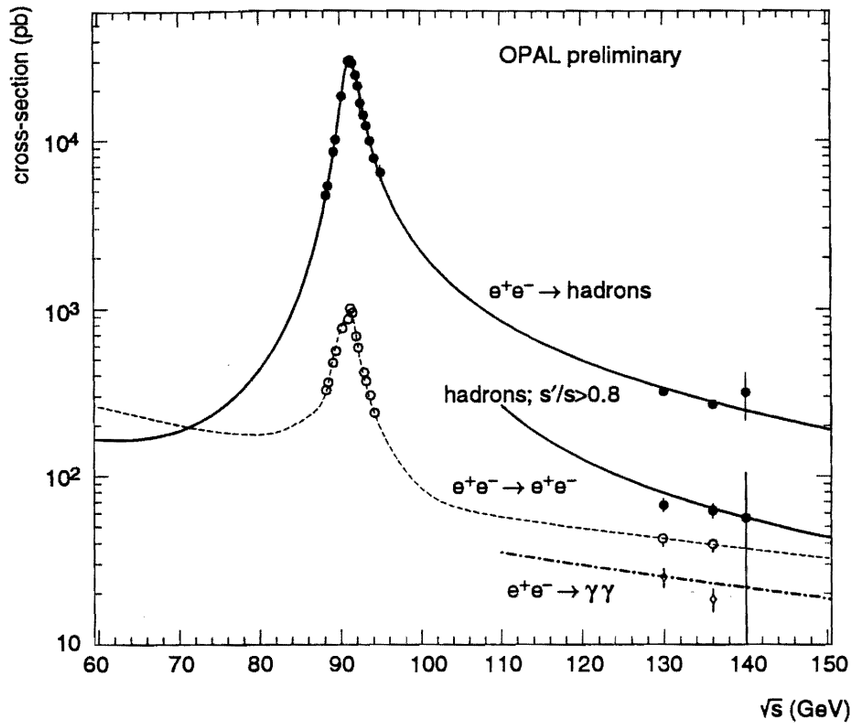

Figure 2: Measured total cross-sections ($s'/s > 0.01$) for various final states from LEP1 and LEP1.5 data. Black points indicate measured multihadron cross-sections, open circles those for $e^+e^-(|\cos\theta_e| < 0.7$, acolinearity $< 10°)$, full triangles $\mu^+\mu^-$, and open diamonds $e^+e^- \to \gamma\gamma$ with the angular cuts described in the text. The curves show the predictions of ZFITTER for multihadrons and muon-pair final states, that of ALIBABA for the e^+e^- final state, and that of an $\mathcal{O}(\alpha^3)$ calculation for the $\gamma\gamma$ final state. For multihadrons and muon pairs, the cross-section expectations and measurements are also shown for $s'/s > 0.8$ at high energies.

$\mu^+\mu^+$ and $\tau^+\tau^-$ final states. These were selected using the criteria optimized at LEP1, which have an efficiency of 83% for $s'/s > 0.01$. The distributions in $\sqrt{s'}$ are shown in Fig. 1c–d for collisions at 130 and 136 GeV, respectively. The non-radiative sample was selected by requiring $s'/s > 0.8$ and corrections were applied for the inefficiency of the selection and the background from lower s'/s values. The cross-sections are shown in Fig. 2. In addition, the average asymmetry at $\sqrt{s} = 133$ GeV was computed and the result is shown in Fig. 3, where it is compared with previous experimental results and with Monte Carlo predictions.

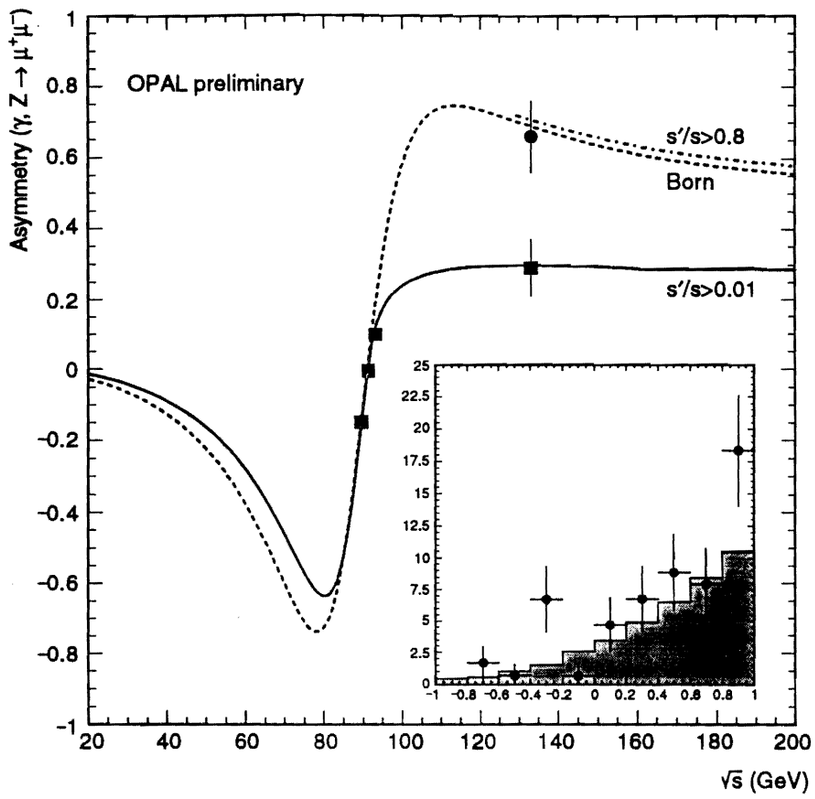

Figure 3: Measured asymmetries for all ($s'/s > 0.01$), and for non-radiative ($s'/s > 0.8$) events as a function of centre-of-mass energy, for muon pairs. The curves show ZFITTER predictions for $s'/s > 0.01$ and $s'/s > 0.8$, as well as the expectation without QED radiative effects, marked 'Born'. The expectation for $s'/s > 0.8$ can lie close to the Born-level curve. The observed distribution of $\cos\theta_{\mu^-}$ in the non-radiative sample is shown in the inset.

The selection of $\tau^+\tau^-$ events at 130–136 GeV is more difficult because of the large background from 2γ-exchange processes. The selection with $s'/s > 0.8$ had an estimated efficiency of about 50%. The average forward–backward asymmetry at $\sqrt{s}$ = 133 GeV for this selection is 0.89 ± 0.11.

$e^+e^- \to \gamma\gamma(\gamma)$ **events**. Here, there are three steps in the selection procedure. The first requires that $E_\gamma/E_{\mathrm{beam}} > 0.2$ and that $15° < \theta_\gamma < 165°$. The second step requires that there is no muon in the detector (to suppress background from cosmic rays and from the beam halo). The third step eliminates events with any charged track from the interaction point. The selected events consist of $e^+e^- \to \gamma\gamma(\gamma)$ as well as $e^+e^- \to \nu\bar{\nu}\gamma\gamma$ events, or are from new physics such as $e^+e^- \to \tilde{\chi}_1^0\tilde{\chi}_1^0\gamma\gamma$. (A good sample of $\nu\bar{\nu}\gamma\gamma$ could be obtained by requiring that the recoil mass to the two photons be larger than 70 GeV). The measured integrated cross-section is shown in Fig. 2, while the angular

distribution is shown in Fig. 4, where it is compared with the QED prediction of $\mathcal{O}(\alpha^3)$ for the accepted kinematic range. The data are consistent with the prediction.

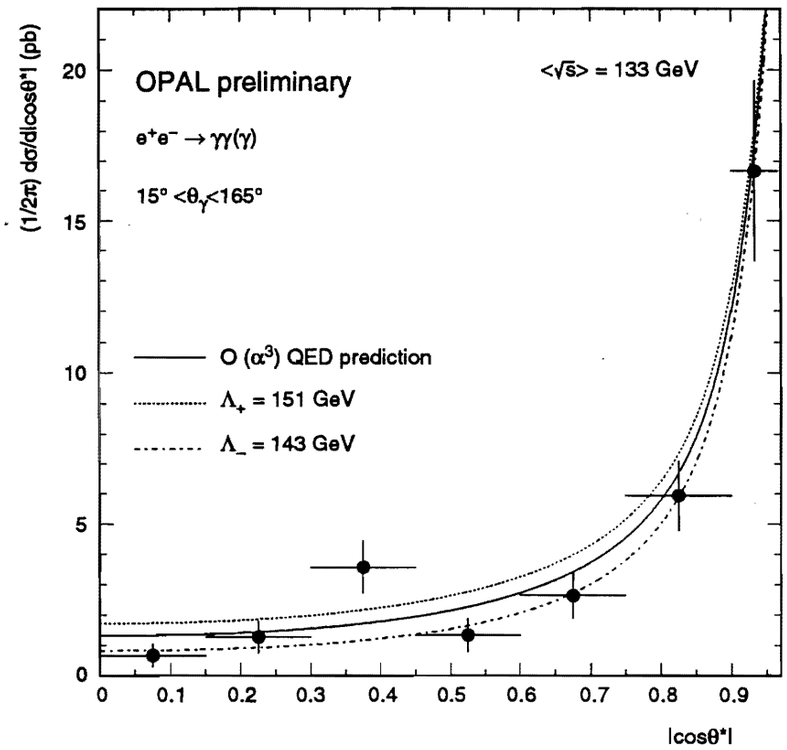

Figure 4: The measured angular distribution for $e^+e^- \to \gamma\gamma(\gamma)$ events. The solid line is the QED prediction at $\mathcal{O}(\alpha^3)$. The evaluated 95% CL lower limits on the cut-off parameters are indicated by dotted (+) and dash-dotted (−) lines.

An indication of the sensitivity of the new data to a cut-off parameter may be obtained assuming that the deviation of the cross-section from the QED prediction is of the type

$$\frac{d\sigma}{d\Omega} = \left(\frac{d\sigma}{d\Omega}\right)_{\text{QED}} \left[1 \pm \frac{s^2}{2\Lambda_\pm^4}(1-\cos^2\theta)\right] . \tag{1}$$

95% CL lower limits on Λ_+ and Λ_- of 151 GeV and 143 GeV, respectively, are obtained. The new data thus represent a test of QED which is as sensitive as the most precise results published at LEP1.

Multiphoton events. These were analysed by the L3 collaboration. The results were consistent with expectations and may be considered another test of QED.

$e^+e^- \to \nu\bar{\nu}\gamma(\gamma)$ **events.** This channel may be selected starting from the analysis described above. A total of 19 events were found in OPAL. The new c.m. energies allow the observation of a highly-energetic photon recoiling against a real Z^0 decaying

invisibly, as discussed in the original 'neutrino counting' proposal. Furthermore this topology is a hunting ground for new physics. The few events obtained are in agreement with the SM predictions.

Electroweak precision measurements. The γ-exchange and Z^0-exchange processes have similar magnitudes at $\sqrt{s} = 130$–140 GeV. OPAL performed a first Z^0-line-shape fit (using the ZFITTER program), which included the new high-energy data, and left the γZ^0 interference term free. It is possible to significantly improve our knowledge of the γZ^0-interference term.

Searches for excited leptons. Searches for excited leptons were performed by the four experiments considering pair production ($e^+e^- \to \gamma \to \ell^*\ell^*$) and single production ($e^+e^- \to \gamma\ \ell^*\ell$), with $\ell = e, \mu, \tau, \nu$, and decays of the type $e^* \to e\gamma$, $\mu^* \to \mu\gamma$, $\tau^* \to \tau\gamma$, $\nu^* \to \nu\gamma$ and $\nu^* \to eW$; no candidates were found. From double pair ℓ^* production the mass limits are at about 57 GeV, while for single ℓ^* production the limits reach $\simeq 130$ GeV.

Two-photon exchange processes. Many events have been collected but no completed analysis is yet available. It is expected that two photon exchange processes will become one of the most interesting areas in the near future.

4. QCD studies

QCD studies have been performed on those multihadronic events which were not subjected to hard initial radiation. These events have been selected with a variety of cuts, for instance $R_{\rm evpm} > 0.5$ and $R_\gamma < 0.4$, where $R_\gamma = E_\gamma/p_\gamma$ is related to the energy and momentum of the observed photons (in $\sim 20\%$ of the cases), while

$$R_{\rm evpm} = \frac{R_{\rm vis} - R_{\rm miss}}{R_{\rm max}} , \tag{2}$$

where

$$R_{\rm vis} = \frac{E_{\rm vis}}{\sqrt{p_\gamma^2 + m_{Z^0}^2}} , \qquad R_{\rm miss} = \frac{P_{\rm miss}}{p_\gamma} , \qquad R_{\rm max} = \frac{2E_{\rm cm}^2}{E_{\rm cm}^2 + m_{Z^0}^2} \tag{3}$$

apply to those cases where the initial state radiated photon is not observed.

The typical numbers of selected events are ~150 at 130 GeV and ~150 at 136 GeV. Studies of event shapes, inclusive charged particle measurements, jet rates, 4 jet analysis, and the evolution of these quantities with energy have been performed with these events.

Event shapes. All event-shape variables (Thrust T, Thrust major $T_{\rm maj}$ and minor $T_{\rm min}$, Oblateness $\mathcal{O}$, Sphericity S, Aplanarity A, etc.) have been studied. For example, the distribution in the Thrust variable, defined as

$$T = \max\left(\frac{\Sigma_1|\vec{p}_1 \cdot \vec{n}|}{\Sigma_1|\vec{p}_1|}\right) , \tag{4}$$

is shown in Fig. 5a. All event-shape variables agree within present uncertainty levels with the JETSET Monte Carlo; some minor retuning of the parameters may have to be made in the future.

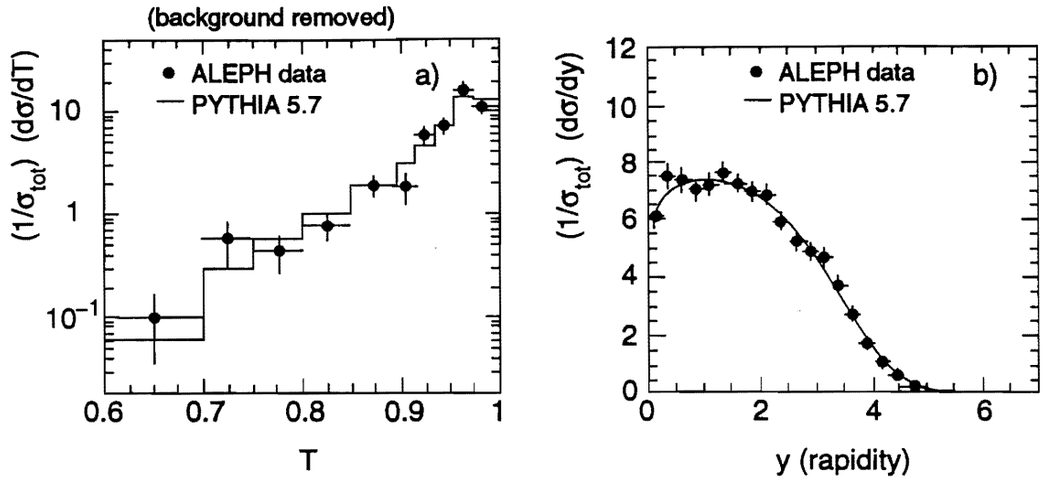

Figure 5: (a) Thrust distribution at the hadron level. (b) Rapidity distribution of charged hadron tracks (130 and 136 GeV data combined, ALEPH).

Inclusive charged particle measurements. These quantities, based on the charged particles of multihadronic events, tend to emphasize QCD phenomena at low energy scales, originating mainly from the radiation of soft gluons.

The *rapidity* distribution is shown in Fig. 5b, where it is compared with the prediction from the PYTHIA Monte Carlo.

The *fragmentation function* $F = (1/\sigma)(\mathrm{d}\sigma/\mathrm{d}\xi_p)$, with $\xi_p = \ln(1/x_p)$, $x_p = p/E_{\mathrm{beam}} = 2p/\sqrt{s}$, is shown as a function of ξ_p in Fig. 6, where it is compared to some predictions. The peak of the distribution is at $\xi_0 = 3.91 \pm 0.05(\mathrm{stat}) \pm 0.07(\mathrm{syst})$.

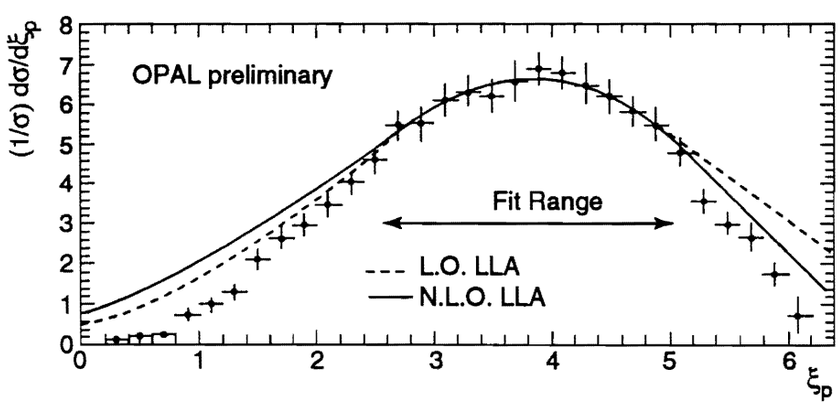

Figure 6: Distribution of charged particles as functions of ξ_p. The fits to determine the position ξ_0 of the peak in the ξ_p distribution are indicated. The solid and dashed lines represent the skewed Gaussian and the normal Gaussian, respectively.

The distribution of the 3-momentum components parallel (p_t^{in}) to the event plane, defined by $\vec{n}_T$ and $\vec{n}_{T_{maj}}$, is shown in Fig. 7.

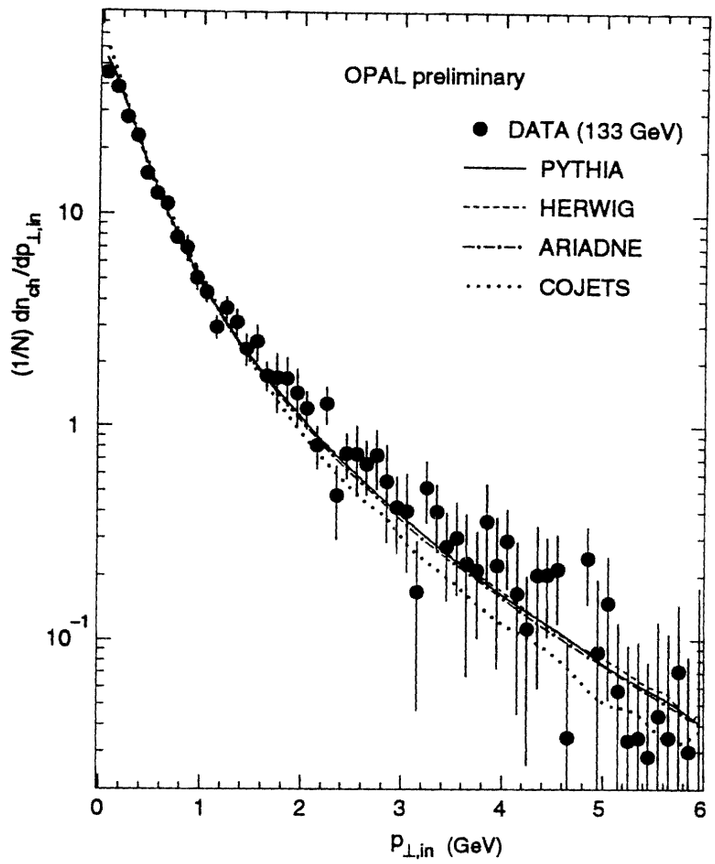

Figure 7: Distribution of the p_t^{in} distribution corrected to the hadron-level for 130 and 136 GeV data combined; superimposed are Monte Carlo predictions.

The corrected *multiplicity distribution* at $\sqrt{s}$ = 133 GeV is shown in Fig. 8. Note that the errors are bin-by-bin correlated because of the correction procedure. The average charged hadron multiplicity is:
OPAL: $\langle n_{ch} \rangle = 23.24 \pm 0.32(\text{stat}) \pm 0.41(\text{syst})$, DELPHI: $\langle n_{ch} \rangle = 23.3 \pm 0.6$.

Figure 9 shows the energy dependence of the mean charged hadron multiplicity. The new value follows the general lower energy trend (even if it is somewhat low) described, for example, by a perturbative QCD formula:

$$\langle n_{ch} \rangle = a\alpha_s^b \exp(c/\sqrt{\alpha_s})(1 + O(\sqrt{\alpha_s})) \ . \tag{5}$$

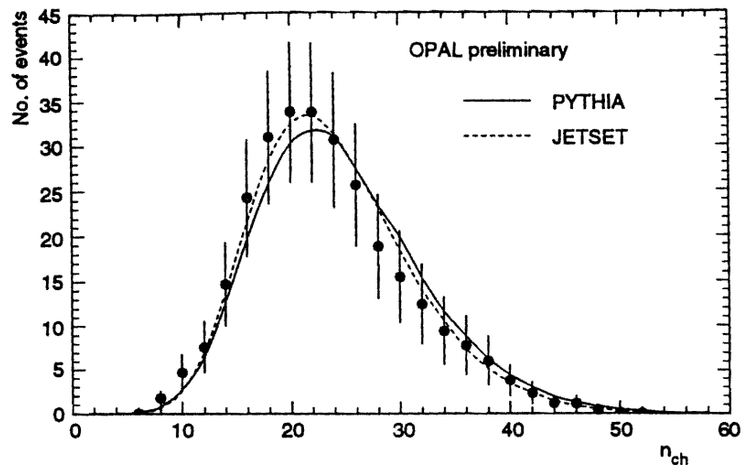

Figure 8: Distribution of the charged particle multiplicity, n_{ch}, for 130 and 136 GeV data combined; the errors shown are statistical only. The errors are correlated between bins because of the correction method. The solid and dashed lines show the predictions from the PYTHIA and JETSET Monte Carlo samples, respectively.

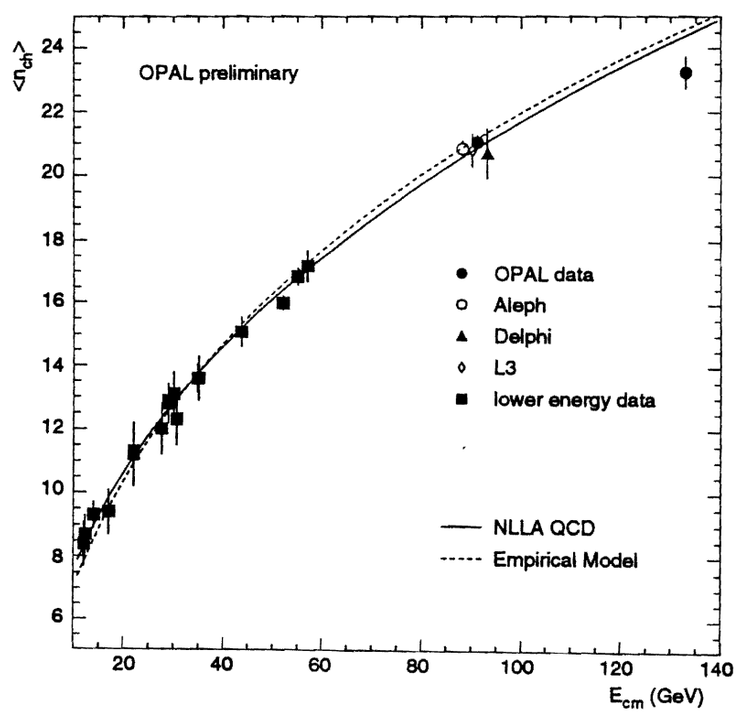

Figure 9: Energy dependence of the mean hadron charged multiplicity.

The *jet rates* at $\sqrt{s} = 136$ GeV are shown in Fig. 10. They have been computed using the JADE scheme E0. In this scheme the invariant mass is defined as

$$m_{ij}^2 = 2E_i E_j (1 - \cos\theta_{ij}) \ , \tag{6}$$

where E_i and E_j are the energies of particles i and j, and $\cos\theta_{ij}$ is the angle between their 3-momentum vectors.

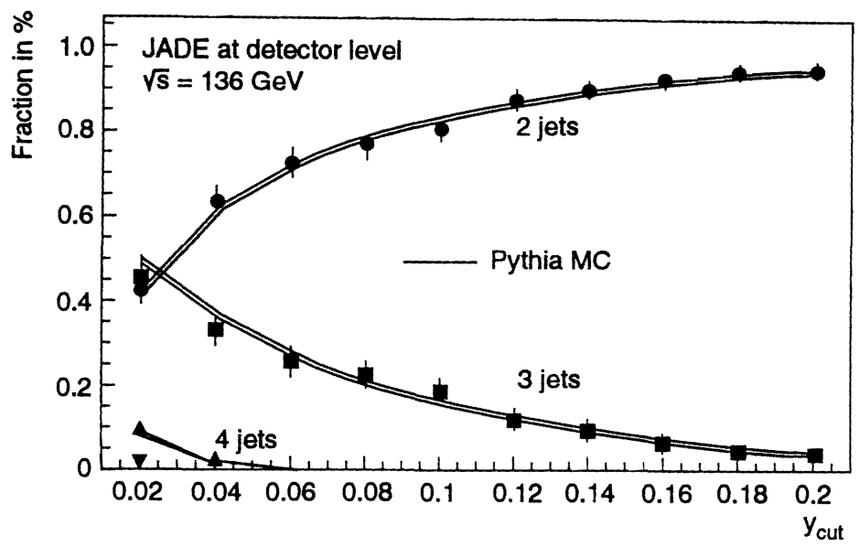

Figure 10: The fractions of 2-, 3-, 4- and 5-jet events as a function of the jet resolution parameter y_{cut} for the E0 JADE scheme (L3).

The energy dependence of the jet rates follows the QCD predictions; a value of α_s can be derived which, with a relatively large error, follows the decreasing trend predicted by QCD.

Other analyses have been started, in particular by the DELPHI Collaboration.

5. Particle searches

5.1. Search for 4-jet final states

This search was mainly motivated by the search of the type $e^+e^- \to h^0 A^0 \to$ 4-jets. The ALEPH Collaboration applied a sequence of selections to their MH sample: (i) $N_{ch} \geq 8$, $E_{ch} > 0.1\sqrt{s}$; (ii) $m_{vis} > 0.7\sqrt{s}$; (iii) using the Durham jet algorithm with $y_{cut} = 0.008$ to find those events with 4 or 5 jets; (iv) remove γ-like jets; (v) energy rescaling, recomputing E_1, E_2, E_3, E_4 and requiring $E_i > 0$; (vi) stricter conditions on 4-jet events: $\min(m_{ij}^{rec}) \geq 25$ GeV, $\min(m_i^{rec} + m_j^{rec}) \geq 10$ GeV, $\min(n_{ch_i} + n_{ch_j}) \geq 10$ (the remaining events have no missing energy); (vii) considering di-jet masses m_{ij} (there are 3 possible pairings), the difference $\Delta m = m_{ij} - m_{k\ell}$, and the sum $\Sigma m = m_{ij} + m_{k\ell}$; (viii) selecting the combination with the smallest mass difference $\min|m_{ij} - m_{k\ell}| \leq 20$ GeV

(this introduces a bias in favour of equal masses, considering a process of the type $e^+e^- \to A + A'$, $A \to (2\text{ jets})_{ij}$, $A' \to (2\text{ jets})_{k\ell}$).

These selections reduced the sample to 14 events, while 7.1 were expected. A plot of these events versus Σm is shown in Fig. 11; it can be seen that in $102 < \Sigma m < 116$ GeV there are 8 events, while 1.35 are expected. The ALEPH Collaboration concludes that there is a fluctuation, which on the basis of known processes has a probability of $\sim 10^{-3}$.

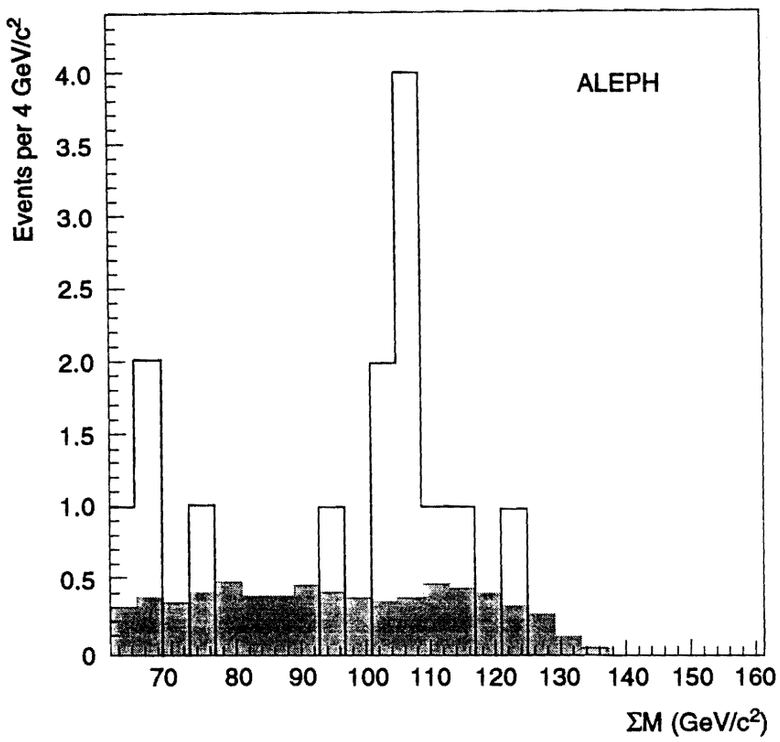

Figure 11: Distribution of 4-jet events plotted against the sum of the masses for the case where the two di-jet masses are approximately equal (ALEPH).

The other collaborations have searched for the same channel (with slightly different cuts, at least at the beginning) and found no fluctuation.

5.2. Study of four-fermion final states

The four-fermion final states, in particular $\ell\bar{\ell}q\bar{q}$, are predicted by the SM, with contributions from different diagrams (see Fig. 12) which vary with energy. Moreover these states may constitute a sizeable background for Higgs searches.

The OPAL Collaboration searched for the $\ell\bar{\ell}q\bar{q}$ events, with guidance from the FERMISV generator which includes the diagrams of Fig. 12 and their interferences; in addition, initial- and final-state photon radiation have been added by hand. The

collaboration found a total of 7 events, 2 $e^+e^-q\bar{q}$ and 5 $\mu^+\mu^-q\bar{q}$ events, while Monte Carlo predictions give 1.2 signal events and 0.5 background events. The excess found (7 ± 1.7) corresponds to a probability of 0.26%.

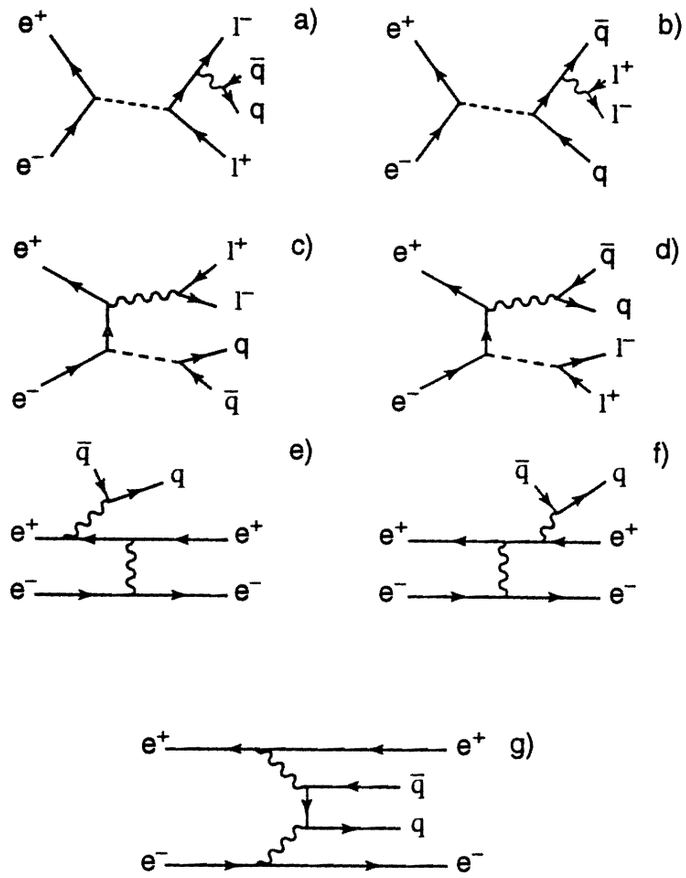

Figure 12: Feynman diagrams for the four-fermion production process $e^+e^- \rightarrow l^+l^-q\bar{q}$: annihilation (a, b), conversion (c, d), Bremsstrahlung (e, f) and multiperipheral (g). The dashed line indicates an intermediate γ or Z^0 boson. The contribution of a diagram increases significantly if the Z^0 boson is on its mass shell. A photon line may be replaced by a Z^0, however on-shell Z^0 bosons are possible only in (a, b) and (e).

5.3. Searches for sypersymmetric particles

Supersymmetry (SUSY) links known particles with super partners, which have identical couplings but whose spin differs by half a unit. Several direct searches performed at LEP1 exclude the existence of supersymmetric particles up to the kinematic limit of $m_{Z^0}/2$, with the exception of the neutralino and gluinos, for which the limits are lower[9]. Indirect limits were also obtained from precision measurements of the

Z^0 lineshape. At LEP1.5 searches were performed for most supersymmetric particles, establishing better limits even with the limited statistics available.

Charginos. Charginos $\tilde{\chi}_1^{\pm}, \tilde{\chi}_2^{\pm}$ are the mass eigenstates corresponding to the linear combinations of charged Higgsinos ($\tilde{H}^{\pm}$) and Winos ($\tilde{W}^{\pm}$). Charginos have been searched for via the pair production process and subsequent decays (see Fig. 13) below:

$$e^+e^- \to \tilde{\chi}^+\tilde{\chi}^-, \qquad \tilde{\chi}^{\pm} \to W^{\pm}\tilde{\chi}^0, \qquad W^{\pm} \to q\bar{q} \quad \text{or} \quad W^{\pm} \to \ell\nu (\text{or } \chi^{\pm} \to \tilde{\nu}\ell^{\pm}) \quad (7)$$

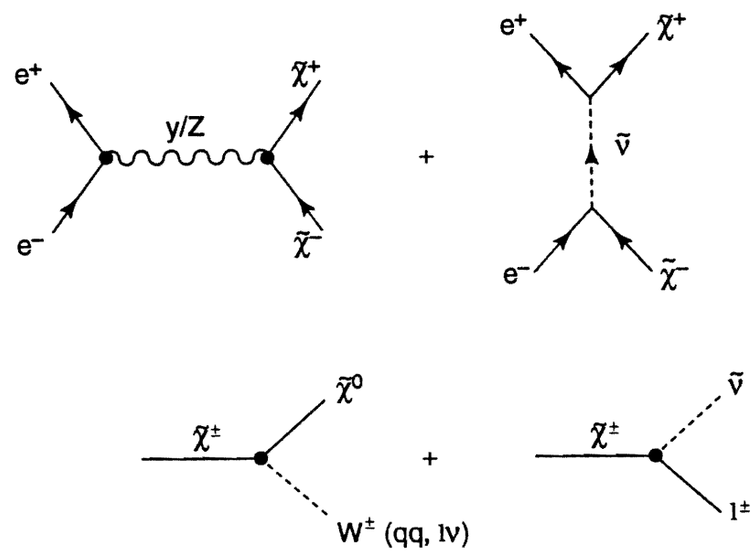

Figure 13: Feynman diagrams for chargino production and decay.

Due to the energies and momenta carried away by the invisible $\tilde{\chi}_1^0$, the experimental signature of $\tilde{\chi}_1^+\tilde{\chi}_1^-$ production is acoplanar pairs of particles or jets, with a large missing momentum. LEP1.5 is below the energy threshold for pair production of real W or Z^0; thus the background to chargino pair production is expected to be small.

Since no chargino candidates have been found upper limits can be placed on the production cross-sections.

Figure 14 gives 95% CL upper limits (independent of the details of the SUSY model) for the production cross-sections for $\tilde{\chi}_1^+\tilde{\chi}_1^-$, assuming specific decay modes. The contours are shown assuming $\tilde{\chi}_1^+ \to W + \tilde{\chi}_1^0$ with 100% BR (solid curves) or $\tilde{\chi}_1^+ \to \ell^+\nu\tilde{\chi}_1^0$ with 100% BR. Thus if the cross-section of $\tilde{\chi}_1^+\tilde{\chi}_1^-$ is larger than 3.5 pb, the existence of charginos with a mass of less than 65 GeV can be excluded at the 95% CL for $\Delta m_+ \geq 10$ GeV, independent of decay mode (up to 68 GeV if $\tilde{\chi}_1^+$ decays via W).

Neutralinos are the four-fermion mass eigenstates $\tilde{\chi}_1^0 - \tilde{\chi}_4^0$ corresponding to linear combinations of $\tilde{\gamma}, \tilde{Z}^0, \tilde{H}_1^0, \tilde{H}_2^0$. Within the context of the Minimal Supersymmetric

Model the previous search can set lower limits at the 95% CL on the chargino and neutralino masses: $m_{\tilde{\chi}_1^0} > 21.4$ GeV, $m_{\tilde{\chi}_2^0} > 33$ GeV, $m_{\tilde{\chi}_1^+} > 65.6$ GeV for $\tan\beta > 1.5$; the limits become 36.9, 67.6 and 65.9 GeV for $\tan\beta = 35$.

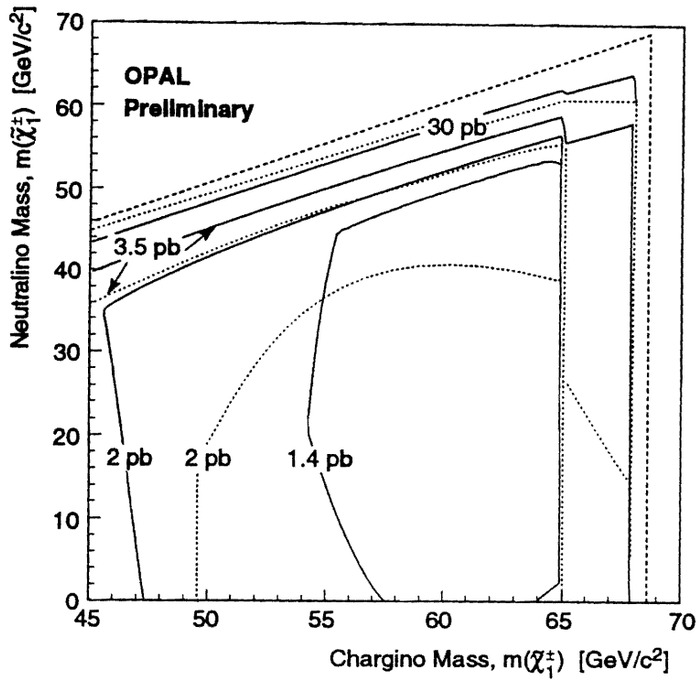

Figure 14: The 95% CL upper limits for the production cross-sections (quoted in pb) for $\tilde{\chi}_1^+\tilde{\chi}_1^-$. The contours of the upper limit are shown, assuming $\tilde{\chi}_1^+ \to W^{*+}\tilde{\chi}_1^0$ with a 100% branching ratio (solid curves) or $\chi_1 \to \ell^+\nu\tilde{\chi}_1^0$ with a 100% branching ratio (dashed curves) (OPAL).

Scalar top quark. L3 reported a search for scalar top via the reaction and decay

$$e^+e^- \to \gamma/Z^0 \to \tilde{t}\tilde{t}, \qquad \tilde{t} \to \tilde{\chi}^0 c\ , \tag{8}$$

From the absence of candidates L3 was able to set the 95% CL limits shown in Fig. 15 for the stop and neutralino masses.

Other searches were performed for sleptons, excited leptons, etc., all with negative results.

6. Conclusions

Data have been collected efficiently by the 4 LEP Collaborations at 130–140 GeV c.m. energy.

All standard fermion pair cross-sections, measured both for all events and after removal of the return to the Z^0, are consistent with expectations. Some cross-sections

can be used to improve the constraints on the interference term in the Z^0 line-shape studies.

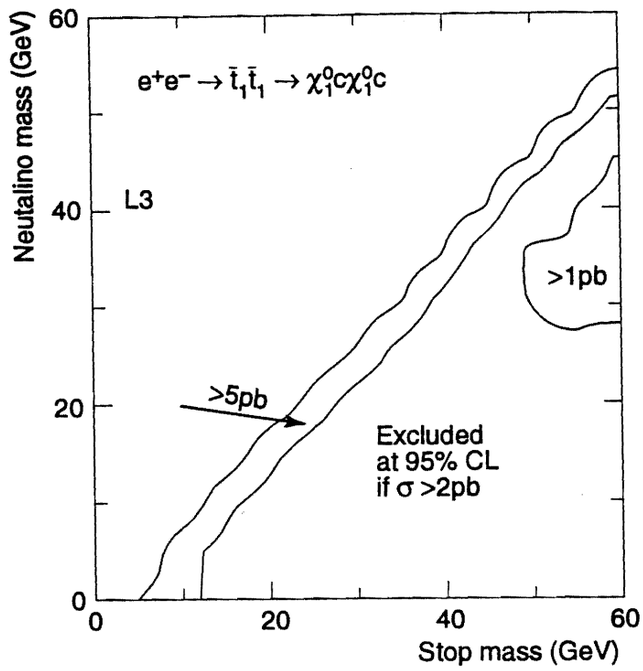

Figure 15: Cross-section limits from the LEP1.5 run as a function of the stop and neutralino masses.

No deviations from QED have been observed and limits for excited leptons have been extended up to $\sim$ 130 GeV.

The lower limits on the mass of neutral heavy leptons have been improved and extended compared to LEP1.

Hadronic event properties and their energy evolution are in agreement with QCD Monte Carlo predictions.

Indications of an excess of events in the 4-jet topology and $\ell^+\ell^-q\bar{q}$ topology need further study.

No evidence has been found for supersymmetric particles (charginos, sleptons, neutralinos, scalar-tops) and limits have been extended compared to those of LEP1.

This glimpse of new data has been exciting and we look forward to LEP2.

Acknowledgments

We would like to thank the members of the four LEP Collaborations for making the material available and for their comments and discussions.

References

1. G. Rolandi, Preliminary results from the 130/136 GeV LEP run with ALEPH, Preprint CERN–95–003, 1995.
2. H. Dijkstra, DELPHI at 130–140 GeV, Preprint CERN–95–004, 1995.
3. G.W. Wilson, First results from the OPAL Collaboration at $\sqrt{s}$ = 130–140 GeV, Preprint CERN–95–005, 1995.
4. D. Stickland, Summary of L3 results from the November 1995 LEP run at 130–140 GeV, Preprint CERN–95–007, 1995.
5. G. Alexander et al., OPAL Collaboration, A study of four fermion final states with high multiplicity at $\sqrt{s}$ = 130–136 GeV at LEP, OPAL Phys. Note PN200 (1996).
   Measurement of cross-sections and asymmetries in e^+e^- collisions at 130–140 GeV c.m. energy, CERN–PPE/96–025 (1996).
   QCD studies with e^+e^- annihilation data at 130 and 136 GeV, OPAL Phys. Note PN–203 (1996).
   Search for chargino and neutralino production using the OPAL detector at $\sqrt{s}$ = 130–136 GeV at LEP, CERN–PPE/96–020 (1996).
   Search for massive particles in 4-jet final states at $\sqrt{s}$ = 130 and 136 GeV with the OPAL detector at LEP, OPAL Phys. Note PN–204 (1996).
   Search for a scalar top quark using the OPAL Detector at $\sqrt{s}$ = 130–136 GeV at LEP, OPAL Phys. Note PN–205 (1996).
   Search for new unstable charged heavy leptons using the OPAL detector at $\sqrt{s}$ = 130 and 136 GeV at LEP, OPAL Phys. Note PN–216 (1996).
   Measurements with photonic events in e^+e^- collisions at c.m. energies of 130–140 GeV, CERN–PPE/96–039 (1996).
6. ALEPH Collaboration, Search for supersymmetric particles in e^+e^- collisions at c.m. energies of 130 and 136 GeV, CERN–PPE/96–10 (1996).
   QCD studies at 130/136 GeV, ALEPH 96–019 (1996).
   Study of $q\bar{q}\ell^+\ell^-$ final states at $\sqrt{s}$ = 130/136 GeV, ALEPH 96–027 (1996).
7. DELPHI Collaboration, Charged particle multiplicity in e^+e^- interactions at $\sqrt{s}$ = 130 GeV, CERN–PPE/96–05 (1996).
8. L3 Collaboration, Studies of hadronic event structure and α_s determination at $\sqrt{s}$ = 130, 136 GeV, CERN–PPE/95–192 (1995).
   Search for excited leptons in e^+e^- annihilations at $\sqrt{s}$ = 130–140 GeV, CERN–PPE/95–190 (1995).
   Measurement of hadron and lepton-pair production at 130 GeV $< \sqrt{s} <$ 140 GeV at LEP, CERN–PPE/95–191 (1995).
   Search for supersymmetric particles at 130 GeV $< \sqrt{s} <$ 140 GeV at LEP, CERN–PPE/96–029 (1996).
9. G. Giacomelli and P. Giacomelli, Particle searches at LEP, Rivista del Nuovo Cimento **16** (1993) 1.